International Journal of Pharmaceutics 662 (2024) 124511

Contents lists available at ScienceDirect

International Journal of Pharmaceutics

journal homepage: www.elsevier.com/locate/ijpharm

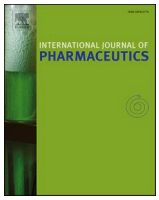

Inhalable dry powders of a monoclonal antibody against SARS-CoV-2 virus made by thin-film freeze-drying

Haiyue Xu [a,1], Sawittree Sahakijpijarn [b,1], Chaeho Moon [a], Christopher J. Emig [c], Marco Mena [c], Steven J. Henry [c], Adela Vitug [c], Christian John Ventura [c], Philip J. Kuehl [d], David Revelli [d], Donald E. Owens III [b], Dale J. Christensen [b], Robert O. Williams III [a,*], Zhengrong Cui [a,*]

[a] The University of Texas at Austin, College of Pharmacy, Division of Molecular Pharmaceutics and Drug Delivery, Austin, TX, 78712, United States
[b] TFF Pharmaceuticals, Inc., Austin, TX, 78746, United States
[c] Augmenta Bioworks, 3475 Edison Way, Suite K, Menlo Park, CA 94025, United States
[d] Lovelace Biomedical, Albuquerque, NM 87108, United States

ARTICLE INFO

Keywords:
Monoclonal antibody
Powder
Lung delivery
Freeze-drying
Viral infection

ABSTRACT

Monoclonal antibodies (mAbs) represent a promising modality for the prevention and treatment of viral infections. For infections that initiate from the respiratory tract, direct administration of specific neutralizing mAbs into lungs has advantages over systemic injection of the same mAbs. Herein, using AUG-3387, a human-derived mAb with high affinity to the severe acute respiratory syndrome coronavirus 2 (SARS-CoV-2) and its various variants, as a model mAb, we formulated the mAb into dry powders by thin-film freeze-drying, confirmed that the AUG-3387 mAb reconstituted from the dry powders retained their integrity, high affinity to the SARS-CoV-2 spike protein receptor binding domain (RBD), as well as ability to neutralize RBD-expressing pseudoviruses. Finally, we showed that one of the AUG-3387 mAb dry powders had desirable aerosol properties for pulmonary delivery into the lung. We concluded that thin-film freeze-drying represents a viable method to prepare inhalable powders of virus-neutralizing mAbs for pulmonary delivery into the lung.

1. Introduction

Monoclonal antibodies (e.g., Humira, Keytruda) have proven effective in various therapeutical areas, including oncology, rheumatology, and infectious diseases. They are predominately developed as a solution or frozen solution for subcutaneous or intravenous injection. For infectious diseases that initiate by viral infection in the respiratory tract, such as influenza viruses, respiratory syncytial viruses (RSV), and SARS-CoV-2, administering pathogen-specific mAbs into the lung holds promise in prevention and treatment of the viral infections (Brainerd et al., 2023; Crowe et al., 1998; Crowe et al., 1994; Detalle et al., 2016; Hermet et al., 2023; McBride et al., 2017; Piepenbrink et al., 2021; Prince et al., 1987; Seow et al., 2023; Leyva-Grado et al., 2015). In reported studies wherein specific mAbs, fragments of antigen-binding (Fabs), or nanobodies were administered into the lung, they were generally dissolved into a solution for nasal or oral inhalation (e.g., intranasal dosing to animals under anesthesia, facial jet or vibrating mesh nebulization to human subjects or non-human primates [NHP]) (Brainerd et al., 2023; Crowe et al., 1998; Crowe et al., 1994; Detalle et al., 2016; Hermet et al., 2023; McBride et al., 2017; Piepenbrink et al., 2021; Prince et al., 1987; Seow et al., 2023; Leyva-Grado et al., 2015). An alternative to nebulization of liquid formulations is oral inhalation of inhalable dry powders directly into the lung using a dry powder inhaler (DPI). Pulmonary delivery by oral inhalation of dry powders has advantages including ease of storage and handling and increased stability of the products, convenience to patients, avoidance of shearing associated with nebulization, and often high delivery efficiency (i.e., the percentage of active ingredient being delivered into the lung). Moreover, unlike liquid, dry powders afford a dissolution step upon administration, which can be modified as needed.

Although there are techniques, such as spray-drying and spray freeze-drying, that can be used to prepare inhalable dry powders of mAbs (Hufnagel et al., 2022a), thin-film freeze-drying (TFFD) represents another particle engineering technology suitable for producing inhalable dry powders (Hufnagel et al., 2022b). TFFD offers potential

* Corresponding authors.
E-mail addresses: bill.williams@austin.utexas.edu (R.O. Williams), Zhengrong.cui@austin.utexas.edu (Z. Cui).
[1] Contributed equally.

https://doi.org/10.1016/j.ijpharm.2024.124511
Received 27 April 2024; Received in revised form 21 July 2024; Accepted 22 July 2024
Available online 25 July 2024

advantages over spraying-based methods. This technology involves rapidly cooling the active pharmaceutical ingredients such as mAbs in a solution along with appropriate excipients (Moon et al., 2019), followed by sublimation to remove water or other solvents (Moon et al., 2019; Sahakijpijarn et al., 2020). Unlike spraying-based methods, TFFD does not require an atomization step, thereby minimizing shear stress and air–liquid interface, which could otherwise damage the mAbs during particle engineering. Moreover, TFFD employs ultra-rapid freezing (typically between 100 and 1000 K/s), minimizing precipitation and particle growth of dissolved solutes (Overhoff et al., 2009). This process generally results in low-density brittle matrix powders (Wang et al., 2014), with desirable characteristics such as high porosity, brittleness, and low bulk density. These powders can be efficiently sheared into respirable low-density microparticles using a DPI device when inhaled by patients (Watts et al., 2013). Currently, two products utilizing this technique are undergoing clinical testing for pulmonary indications (NCT04872231 and NCT04576325). While Hufnagel et al. recently demonstrated the feasibility of applying TFFD to produce respirable dry powders of mAbs, such as anti-PD-1 and anti-TNF-α mAbs (Hufnagel et al., 2022b), no study has yet investigated the activity of mAbs in powders prepared using the TFFD method.

In the present study, we developed dry powder formulations of AUG-3387 (Emig et al., 2021), a human-derived mAb that binds to SARS-CoV-2 spike protein for pulmonary delivery using TFFD. We characterized the physical and aerosol properties of the powders as well as the activity of the mAbs upon reconstitution. We also tested the feasibility of delivering one of the mAb powders directly in the lung by dry powder insufflation in a Syrian (golden) hamster model for potential neutralization of SARS-CoV-2 virus.

SARS-CoV-2 is the causative agent of coronavirus disease 2019 (COVID-19). The virus infects the upper respiratory tract first, with the nasal cavity being the dominant initial site, and then spreads into the deep lungs if not being successfully challenged by the host's immunity (Hou et al., 2020). In the lungs, the virus gains entrance to the epithelial cells by interacting with the angiotensin-converting enzyme (hACE2) receptor expressed on the surface of the cells via the RBD of the spike protein of the virus, and from there spreads to other parts of the host's body (Xu et al., 2020). During the COVID-19 pandemic, several anti-SARS-CoV-2 mAb products were granted Emergency Use Authorization, but all were administered by infusion or injection, which include Casirivimab and Imdevimab by Regeneron Pharmaceuticals (Tarrytown, NY), Bamlanivimab and Etesevimab by Eli Lilly (Indianapolis, IN), and Sotrovimab by GSK (Brentford, United Kingdom) in partnership with Vir Biologics (San Francisco, CA) (Yu et al., 2023). Although generally limited to infusion centers and out-patient settings, those mAbs have proven effective in reducing hospitalization in mild to moderate COVID-19 patients (Gupta et al., 2021; Weinreich et al., 2021; Chen et al., 2021). As to the efficacy of SARS-CoV-2 mAbs given by inhalation, Hermet et al. (2023) reported that compared to intravenous injection, higher antibody concentrations were achieved in the lungs of NHPs treated with an mAb via vibrating mesh nebulization, resulting in more viral load reduction in the lungs post viral infection (Hermet et al., 2023). Similarly, Streblow et al. (2023) reported that nebulization of a SARS-CoV-2 mAb in macaques reduced viral RNA and infectious viruses in the upper and lower respiratory tracts (Streblow et al., 2023). Finally, antibodies against SARS-CoV-2 were also tested in human subjects by nebulization (Maranda et al., 2024). The AUG-3387 mAb used in the present study was isolated using Augmenta Bioworks' SingleCyte® system and was shown to display high affinity to the SARS-CoV-2 spike protein (Emig et al., 2021). AUG-3387 also demonstrated strong binding to the Alpha, Beta, Gamma, Delta, Lamda and Mu variants of SARS-CoV-2 (Emig et al., 2021). Furthermore, the mAb's neutralization activity validated that the binding is on a site that prevents the virus from binding the hACE2 receptor (Emig et al., 2021).

2. Materials and methods

2.1. Materials

AUG-3387 IgG1 was produced in HEK293 cells by Absolute Antibody (Oxford, UK) or in CHO cells by Catalent (Somerset, NJ) after discovery, design and cloning at Augmenta Bioworks (Menlo Park, CA) (Fig. 1). D-mannitol, D-trehalose, leucine, polysorbate 20, sodium chloride, sodium phosphate dibasic, Dulbecco's phosphate-buffered salt solution (DPBS, 1x), Zeba Spin Desalting Columns (7 K MWCO, 0.5 mL), and acetonitrile (HPLC grade) were from Thermo-Fisher Scientific (Pittsburgh, PA). SARS-CoV-2 Wuhan-1 RBD, B.1.1.17 (Alpha) S1, 20H/501Y.V2 (Beta) S1, B.1.617.2 (Delta) RBD, B.1.1.28 (Gamma) S1 + S2, B.1.617 (Kappa) RBD, and K417T, E484K, N501Y RBD were from Sino Biological US Inc. (Wayne, PA). SARS-CoV-2 Lenti Pseudovirus that expresses luciferase was from GenScript (Piscataway, NJ). Bovine serum albumin (BSA) was from Rockland Immunochemicals, Inc. (Pottstown, PA). HEK293T cells were from the American Type Culture Collection (Manassas, VA). The pCMV-AC-GFP Ace2 expression vector was from Origene (Rockville, MD). ACE2 polyclonal antibody was from Proteintech (Rosemont, IL). MagPlex-C microspheres, antibody conjugation Kit, and 1x MAP Sheath Fluid (20 L, RUO) were from Luminex Co. (Austin, TX). Goat anti-human IgG/IgA/IgM F(ab')2 PE was from Sigma-Aldrich (St. Louis, MO). Anti-V5 antibody clone SV5-Pk1 was from Abcam (Waltham, MA). Bright-Glo™ Luciferase Reagent was from Promega (Madison, WI). Experion™ Pro260 Analysis Kit was from Bio-Rad Laboratories (Hercules, CA). The High-resistance Monodose RS00 dry powder inhalers were generously provided by Plastiape S.p.A. (Osnago, Italy).

2.2. Preparation of thin-film freeze-dried AUG-3387 powders

To prepare the solutions for thin-film freezing, AUG-3387 that was in phosphate-buffered saline (PBS) was combined with excipients as shown in Table 1. Then the solutions were passed through 0.45 μm polyethersulfone (PES) syringe filters. The solution was dropped onto a rotating stainless steel drum surface that was cryogenically cooled by liquid nitrogen to −70 to −80 °C. The frozen solids were collected and stored in a −80 °C freezer before drying in the lyophilizer. The drying step was performed using an SP VirTis Advantage Pro shelf lyophilizer (SP Industries, Inc., Warminster, PA). During drying cycle, the frozen samples were held at −40 °C for 20 h, then ramped to 25 °C over 20 h, and finally held at 25 °C for 20 h. The pressure was maintained at 100 mTorr during the drying cycle (Hufnagel et al., 2022b).

2.3. Target binding characterization

SARS-CoV-2 S1 RBD proteins and various other antigens and controls were covalently coupled to Luminex MagPlex magnetic microspheres to measure mAb-antigen binding with a Luminex 200 instrument (Austin, TX). The following antigens were conjugated: SARS-CoV-2 Wuhan-1 RBD, B.1.1.17 (Alpha) S1, 20H/501Y.V2 (Beta) S1, B.1.1.28 (Gamma) S1 + S2, B.1.617.1 (Kappa) RBD, K417T/E484K/N501Y RBD, and BSA. Each antigen was conjugated with the xMAP conjugation kit at ratio of 5 μg protein to 1 million beads according to the manufacturer's recommended protocol. Assays were performed in multiplex, with each spectrally encoded bead having a separate antigen and run together in a single well. Antibody was titrated over therapeutically relevant concentrations, mixed with the beads, washed twice, labeled with an anti-human IgG/IgA/IgM F(ab')2 PE secondary antibody, washed twice and run on the instrument. The TFF AUG-3887 powders were reconstituted in water before dilution for the binding assay.

2.4. Pseudovirus neutralization assay

An ACE2 expressing HEK293T cell line ("LentiX ACE2.S4") was constructed by packaging pCMV-AC-GFP into Lentivirus and

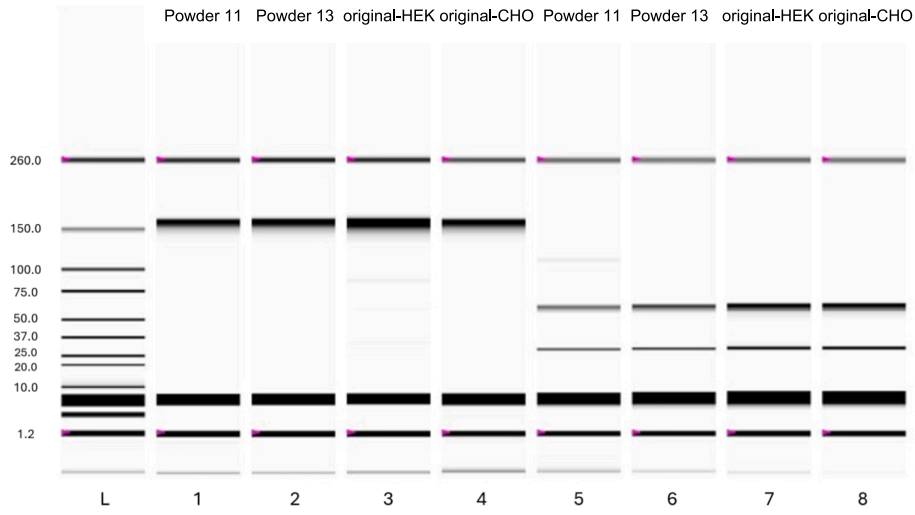

Fig. 1. Bio-Rad Experion virtual gel images of AUG-3387 mAbs reconstituted from TFF AUG-3387.11 or AUG-3387.13 powders of CHO-expressed antibody (native in lanes 1 and 2, reducing in lanes 5 and 6) and AUG-3387 mAbs as expressed in HEK293T cells (native in lane 3 and reduced in lane 7) or CHO cells (native in lane 4 and reduced in lane 8).

Table 1
Compositions of TFF AUG-3387.11 and AUG-3387.13 formulations.

Formulation	Composition (% w/w)						Solid content (% w/v)
	AUG-3387	Sodium phosphate	Sodium chloride	Mannitol	Trehalose	Leucine	
AUG-3387.11	13.70	1.604	8.578	72.31	–	3.81	1.0
AUG-3387.13	13.70	1.604	8.578	–	72.31	3.81	1.0

Note: The weight percentages were calculated numbers. Samples were prepared by dissolving AUG-3387, mannitol or trehalose, and leucine in a PBS buffer to reach a solid content of 1% (w/v).

transducing HEK293T cells. The cells were enriched via flow cytometry on an SH800 cytometer (Sony Biotechnologies, San Jose, CA) four times until 97 % of the cells showed signal above the negative control as read out by staining with anti-ACE2 and secondary antibodies. The final enriched ACE2-HEK293T cells had approximately 50× the secondary fluorescence signal of non-transduced cells. For the SARS-CoV-2 Pseudovirus neutralization assay, two days prior to infection, LentiX ACE2. S4 cells were grown to 85 % confluency, seeded in a 96-well plate at 15,000 cells/well in 50 μL media per well, and then held at 37 °C in 5 % CO_2 until infection. Antibody mixtures were created prior to infection by performing a 128-fold serial dilution starting at 40 μg/μL. AUG-3387 reconstituted from TFF powders and soluble negative control anti-V5 Tag mAb were added in triplicate, and the original AUG-3387 solution was added in duplicate. SARS-CoV-2 Wuhan-1 pseudoviruses were diluted in Dulbecco's Modified Eagle Medium (DMEM) to 3.2×10^7 IFU/mL, and 100 μL of virus solution was mixed with 100 μL of diluted antibody. The virus/antibody mixture was incubated for 60 min at 37 °C in 5 % CO_2. Following incubation, 50 μL of the pseudovirus/antibody mixture was added to each well of seeded cells. Additional controls included cells only and cells with viruses only. After 48 h, the plate was removed and equilibrated at room temperature for 10 min, and 60 μL of the supernatant was removed. Then 50 μL of Promega's Bright-Glo Luciferase assay reagent was added to each well of the infected cells. The cells were incubated at room temperature for 3 min, and luminescence was measured with a Tecan Life Sciences' Spark multimode microplate reader (Mannedorf, Switzerland) in luminescence mode with a 1 s integration time.

2.5. Aerodynamic particle size distribution analysis

About 3–5 mg of AUG-3387 mAb dry powder was loaded into size #3 hydroxypropyl methylcellulose (HPMC) capsules (Vcaps® plus, Capsugel®, Lonza, Morristown, NJ). The aerodynamic properties of the powder were evaluated using a Next Generation Impactor (NGI) (MSP Corporation, Shoreview, MN) connected to a High-Capacity Pump (model HCP5, Copley Scientific, Nottingham, UK) and a Critical Flow Controller (model TPK 2000, Copley Scientific). The dry powder inhaler device Plastiape® RS00 was used for dispersing the powder through the USP induction port with a total flow rate of 60 L/min for 4 s per each actuation, corresponding to a 4 kPa pressure drop across the device and a total flow volume of 4 L. To avoid particle bounce, a solution of polysorbate 20 in methanol at 1.5 % (w/v) was applied and dried onto the NGI collection plates to coat their surface. The pre-separator was not used in this analysis. After dispersal, the powders were recovered from the stages, and the samples were analyzed using HPLC-ELSD as described below. The analysis was conducted three times (n = 3). The NGI results were analyzed using the Copley Inhaler Testing Data Analysis Software 3.10 (CITDAS). CITDAS provided the calculation for mass median aerodynamic diameter (MMAD), geometric standard deviation (GSD), fine particle fraction (FPF) of delivered dose (FPF%, delivered) and recovered dose (FPF%, recovered). The FPF of delivered dose was calculated as the total amount of sugar or sugar alcohol (e.g., trehalose, mannitol) collected with an aerodynamic diameter below 5 μm as a percentage of the total amount of sugar or sugar alcohol deposited on the adapter, the induction port, stages 1–7 and Micro-orifice collector (MOC).

2.6. Excipient quantification by HPLC – ELSD

The quantitation of main excipients (e.g., mannitol, trehalose) in the deposited powders after NGI testing was performed using an Agilent® 1260 Infinity II HPLC (Agilent, Santa Clara) equipped with an Agilent® 1290 Infinity II ELSD. The evaporation and nebulization temperature were set at 60 °C. The gas flow rate was maintained at 1.6 L/min. The

mobile phases were water (A) and acetonitrile (B). The gradient method was performed for 6 min with a flow rate of 1 mL/min (0 min, 20 % A and 80 % B; 0.5 min, 20 % A and 80 % B; 3.3 min 60 % A and 40 % B; 3.5 min, 60 % A and 40 % B; 3.6 min, 20 % A and 80 % B; and 6 min, 20 % A and 80 % B). A Waters XBridge® Amide Column (4.6 × 150 mm, 3.5 μm) (Waters, Milford, MA) was used at 30 °C and a flow rate 1.0 mL/min. The injection volume was 15 μL. All chromatograms were processed using an Agilent® Open Lab CDS software.

2.7. Microfluidic capillary gel electrophoresis

CHO-expressed AUG-3387 dry powder formulations AUG-3387.11 and AUG-3387.13 were resuspended in water and diluted to 500 ng/μL with PBS. AUG-3387 expressed in CHO and AUG-3387 expressed in HEK-293 T cells were diluted to 500 ng/μL with PBS. Four microliters of each sample were processed with the Experion Pro260 Analysis Kit (700–7101) in both reducing and non-reducing conditions and analyzed on an Experion System (700–7000) according to the manufacturer's recommended protocol.

2.8. X-ray diffraction (XRD)

XRD was conducted using a Ragaku Miniflex 600 II equipped with primary monochromated radiation (Cu K radiation source, $\lambda = 1.54056$ Å). The instrument was operated at an accelerating voltage of 40 kV at 15 mA. Samples were loaded in the sample holder and scanned in the range of 5–40 Å of 2θ at a scan speed of 2 °C/min, a step size of 0.02 °C/s, and a dwelling time of 2 s.

2.9. Modulated differential scanning calorimetry (mDSC)

Thermal analysis of TFF powders was carried out with a DSC model Q20 (TA Instruments, New Castle, DE) equipped with a refrigerated cooling system (RCS40, TA Instruments) under dry nitrogen gas at a flow rate of 50 mL/min. The samples were accurately weighed and loaded into Tzero pans. The pans were hermetically sealed with Tzero hermetic lids. A hole was made on the lid before placing the pan in the sample holder. Modulated DSC was performed with a modulation period of 60 s, modulated amplitude of 1 °C. The samples were equilibrated at 25 °C, and cooled down to −30 °C at a rate of 10 °C/min. Then the samples were heated at a heating ramp rate of 5 °C/min over a temperature range of −30 °C–250 °C. Data of the heating step was processed using a TRIOS software.

2.10. Specific surface area (SSA) measurement

The SSA of the powder was measured using an AutoFlow BET+surface analyzer (Quantachrome, Boynton Beach, FL, USA) and the multipoint Brunauer–Emmett–Teller (BET) method. The sample was accurately weighed and outgassed under ultra-high purity grade helium at 50 psi at 30 °C for 20 h before gas adsorption analysis. The outgassing temperature was selected to avoid heat-related degradation of the physical properties of powder while still removing the water vapor. The adsorbate gas was ultra-high purity grade nitrogen. The surface area was calculated using the Quantachrome FloWin™ software.

2.11. Moisture content measurement

The residual moisture content of the TFF powder was analyzed by Coulometric Karl Fisher Titration using a Titrator Compact C10SX (Mettler Toledo, Columbus, OH). The Hydranal™ Coulomat CG-K and AK (Honeywell International Inc., Charlottle, NC) as catholyte and anolyte, respectively, were employed for the coulometric KF titration. At least 10 mg of powder were accurately weighed and transferred into glass serum vials in a glove box that was filled with dry nitrogen gas. About 1 mL of Hydranal™ formamide dry (Honeywell International Inc.) was added into the vials. The vials were sealed with stoppers and aluminum caps. The samples were mixed using a vortex mixer and a sonicator until a clear solution was obtained. A syringe needle was used to transfer the samples from the vials into the KF titration cell. The percentage of moisture content (% w/w) was calculated based on the moisture content (mg) and the sample weight (mg).

2.12. Scanning electron microscopy (SEM)

The TFF powder was placed onto carbon tape and mounted onto aluminum stubs followed by a sputter-coating with platinum/palladium to a thickness of 15 nm (Cressington Scientific Instruments LTd., Watford, UK) before capturing the images using a Zeiss Supra 40 (Carl Zeiss, Oberkochen, Germany).

2.13. Efficacy of AUG-3387 in an in vivo model of SARS-CoV-2 infected Syrian hamsters

An *in vivo* efficacy study was performed using male Syrian Hamsters (*Mesocricetus auratus*) (Charles River Laboratory, Wilmington, MA) approximately 9 weeks of age with a weight range of 110–134 g at the time of randomization. Animal work was performed at the Lovelace Biomedical Research Institute (LBRI) with approval from the Institutional Animal Care and Use Committee and within Animal Biosafety Level 3 (ABSL3) containment. Hamsters were singly housed in filter-topped cage systems and were supplied with a certified diet, filtered municipal water, and dietary and environmental enrichment. The efficacy study design is detailed in Table 2. Animals were assigned to groups (n = 6) using a stratified (body weight) randomization procedure. All animals were euthanized at the end point with a solution consisting of 390 mg of sodium pentobarbital and 50 mg of phenytoin per mL. Lung samples (in Trizol) were stored at −80 °C prior to analysis.

2.13.1. Viral infection

SARS-CoV-2 virus, isolate USA-WA1/2020, was from the World Reference Center for Emerging Viruses and Arboviruses (WRCEVA) (Galveston, TX) and propagated in Vero E6 African Green Monkey kidney cells (BEI, catalog #N596) in DMEM supplemented with 1 % HEPES, 10 % FBS, 100 IU/mL penicillin G and 100 μg/mL streptomycin. Stocks were stored in a BSL-3 compliant facility at −80 °C prior to the challenge. Stock vials of viruses were thawed on the day of infection, diluted as necessary, and stored on ice until use. Viral dose was quantitated using a $TCID_{50}$ assay using the Reed and Muench method on Vero E6 cells in DMEM supplemented with 2 % FBS and 100 IU/mL penicillin G and 100 μg/mL streptomycin (Reed and Muench, 1938). A dose of 1.0×10^5 $TCID_{50}$ per animal was targeted, and the actual dose averaged 5.8

Table 2
Design of the animal study.

	Group description	Infection day	Dose	Route/ Frequency	Study endpoints
1	Vehicle Control	Day 0	N/A	IP; once on day 1	Twice daily clinical observations, body weights daily, necropsy on day 5 for viral load in lung tissues and histopathology
2	mAb powder High dose	Day 0	1.0 mg/kg	IT; once daily on days 1,2,3	
3	mAb powder Low dose	Day 0	0.33 mg/kg	IT; once daily on days 1,2,3	
4	mAb solution High dose	Day 0	10.0 mg/kg	IP; once on day 1	
5	mAb solution Low dose	Day 0	3.3 mg/kg	IP; once on day 1	

IT, intratracheal insufflation of TFF AUG-3387.11 powder; IP, intraperitoneal injection of AUG-3387 in a solution.

$\times 10^5$ $TCID_{50}$ per animal. The viral dose was delivered via intranasal installation under anesthesia (ketamine 80 mg per kg and xylazine 5 mg per kg) with a volume of 100 μL per nare, 200 μL total per animal.

2.13.2. Treatment

The AUG-3387 mAb was delivered by one of two routes for each animal, intratracheal insufflation (IT) or intraperitoneal (IP) injection (Table 2). The IP injection was performed with a 16 mg/mL AUG-3387 solution in saline. The IT insufflation was performed with animals under anesthesia (4–5 % isoflurane with oxygen) until a deep plane of anesthesia was reached. TFF AUG-3387.11 powder was transferred to the ABSL-3 facility, and each Penn Century DP-4 device were quantitatively loaded with the powder. Doses were based on a method developed to quantify the amount of material that exited the devices, assuming 100 % presentation at the terminus of the cannula and the average body weight of the animals at the time of dosing.

2.13.3. Quantitative assessment of viral burden

Quantitation of subgenomic viral RNA by RT-qPCR was used as markers for viral burden. Lung samples were assayed via RT-qPCR for E-gene (subgenomic). Lung samples were weighed and homogenized using a Tissue Lyser (Qiagen, Hilden, Germany) in 1 mL of TRI reagent. RNA was extracted using the Direct-Zol 96-RNA kit (Zymo Research, Orange, CA) according to manufacturer's instructions. Copies of SARS-CoV-2 E gene were measured by qRT-PCR TaqMan Fast Virus 1-step assay (Thermo Fisher). SARS-CoV-2 specific primers and probes from the 2019-nCoV RUO Assay kit (Integrated DNA Technologies) were used: (L Primer: CGATCTCTTGTAGATCTGTTCTC; R primer: ATATTGCAGCAGTACGCACACA; probe: 6FAM-ACACTAGCCATCCTTACTGCGCTTCG-BHQ-1). Reactions were carried out on a Bio-Rad CFX384 Touch instrument according to the manufacturer's specifications. A semi-logarithmic standard curve of synthesized SARS-CoV-2 E gene RNA (LBRI) was obtained by plotting the Ct values against the logarithm of cDNA concentration and used to calculate SARS-CoV-2 E gene in copies per gram of tissue. Thermal cycling conditions involved 5 min at 50 °C for reverse transcription, followed by an initial denaturation step for 20 s at 95 °C and 40 cycles of 95 °C for 3 s and 60 °C for 30 s.

2.14. Statistical analyses

All statistical analyses wherein comparisons were made were performed using either one way ANOVA or student's *t*-test with statistical significance defined as $p < 0.05$ and values expressed as mean ± S.D. or S.E.M. For comparison of 3 or more values, ANOVA was used with Neuman-Keuls post hoc test for comparison of values. When two groups were compared, the student's *t*-test was used.

3. Results and discussion

In the present study, we formulated the AUG-3387, a human-derived mAb against SARS-CoV-2 spike protein as a model mAb, into TFF powders, characterized the dry powders and the mAb in the powders, evaluated the activity of the AUG-3387 in the powders, and tested the feasibility of administering one of the mAb powders into the lungs of Syrian hamsters by intratracheally insufflation for potential prevention or treatment of SARS-CoV-2 viral infection.

3.1. Formulation and characterization of TFF AUG-3387 powders

Initially, we prepared a series of TFF AUG-3387 powders containing various concentrations of AUG-3387 (e.g., 5–20 %, w/w) and different excipients (e.g., lactose, trehalose, mannitol, leucine, salts as in PBS). The powders were then screened based on examining the reconstituted samples for mAb integrity by SDS-PAGE or microfluidic capillary gel electrophoresis and for the absence of significant subvisible aggregates as examined under a light microscope. TFF AUG-3387.11 and AUG-3387.13 (Table 1), which showed the least amounts of subvisible aggregates upon reconstitution, were selected for additional studies.

The AUG-3387 mAbs reconstituted from TFF AUG-3387.11 and AUG-3387.13 powders were virtually identical to the original AUG-3387 mAb in a solution in microfluidic capillary gel electrophoresis image (Fig. 1), indicating that subjecting AUG-3387 to the TFFD process did not cause fragmentation of the mAb. Similarly, in an experiment evaluating the binding affinity of the AUG-3387 mAb to the spike proteins or RBDs of SARS-CoV-2 Wuhan-1 and other variants, i.e., B.1.1.17 (Alpha), 20H/501Y.V2 (Beta), B.1.1.28 (Gamma), B.1.617.1 (Kappa), and K417T/E484K/N501Y, the AUG-3387 mAbs reconstituted from the TFF AUG-3387.11 and AUG-3387.13 powders performed essentially identically as the original AUG-3387 in a solution (Fig. 2). Moreover, in a neutralization assay with pseudoviruses that expressed SARS-CoV-2 Wuhan-1 RBD, the AUG-3387 mAbs reconstituted from the TFF AUG-3387.11 and AUG-3387.13 powders and the original AUG-3387 in a solution did not show any significant difference (Fig. 3). It was thus concluded that the integrity, binding affinity, and virus neutralizing activity of the AUG-3387 mAbs in the TFF AUG-3387.11 and AUG-3387.13 powders were not significantly different from that in the original AUG-3387 in a PBS solution.

3.2. Aerosol performance of TFF AUG-3387 powders

The aerosol properties of the TFF AUG-3387.11 and TFF AUG-3387.13 powders were analyzed using NGI. The TFF AUG-3387.11 powder demonstrated desirable aerosol properties (see Fig. 4 for example). The MMAD value was 3–4 μm, with FPP delivered at around 50 % (Table 3). In another independent study, the AUG-3387.11 powder showed an MMAD value of 1.7 μm and an FPF (delivered) value of ~80 %, likely due to lower relative humidity when the experiment was done. The TFF AUG-3387.13 powder, however, did not show good aerosol properties, with over 70 % of the powder deposited in the S1 stage of the NGI device. Therefore, the TFF AUG-3387.11 powder was used for additional studies. It is noted that the Plastiape RS00 high resistance device used to measure the aerosol properties of the TFF AUG-3387 powders is designed to provide maximum shear and aerosolization of powders at low airflow rates and is ideal for delivery into the deep lung of patients with reduced lung function (e.g., after a viral infection).

3.3. Physical properties of the TFF AUG-3387.11 powder

The surface morphology, specific surface area, and moisture content of the TFF AUG-3387.11 powder were examined/measured. Fig. 5 shows representative SEM images of the AUG-3387.11 powder with irregular shape particles. The specific surface area of the AUG-3387.11 powder was 19.44 ± 9.65 (m^2/g), and the residual moisture content in it was 3.14 ± 0.60 % (w/w). The crystallinity of the TFF AUG-3387.11 powder was characterized using XRD and mDSCs. Individual excipient was prepared as TFF neat excipient powder and characterized for crystallinity. XRD diffractograms showed that sodium chloride, sodium phosphate, mannitol, and leucine were all crystalline after being subject to TFFD, both as individual neat components and as part of the mAb powder (Fig. 6). XRD demonstrated the sharp peaks of delta-mannitol (9.5, 19.3, 20.5, 21.1, 22.1, 24.6,25.3, 27.8, 35, 36.1 degrees) and sodium chloride (31.7 degree) in the TFF AUG-3387.11 powder and its placebo; however, leucine peaks were not observed (Fig. 6). Since the amount of leucine in the TFF AUG-3387.11 powder was lower than 5 %, it is possible that XRD was not able to detect leucine peaks due to the limit of the XRD detection. Thermal behaviors and crystallinity of the TFF AUG-3387.11 powder were further analyzed using mDSC, which showed that TFF neat mannitol and leucine powders were crystalline (Fig. 7). TFF neat mannitol showed a melting point at ~162 °C. No glass transition temperature (Tg) was observed in the TFF AUG-3387.11 powder. Interestingly, the TFF AUG-3387.11 formulation showed two melting points of mannitol at ~139 °C and ~151 °C (Fig. 7),

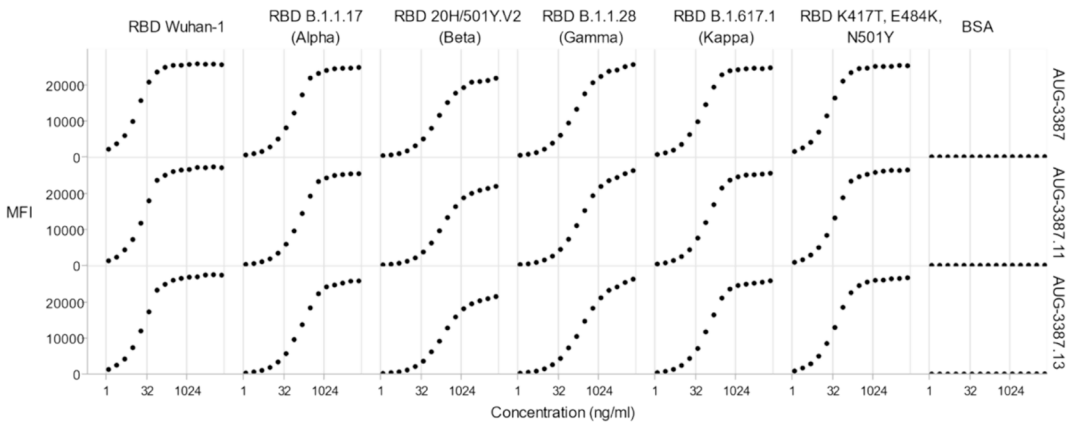

Fig. 2. Binding of AUG-3387, original in a PBS solution or reconstituted from TFF AUG-3387.11 or AUG-3387.13 powders, to RBDs of SARS-CoV-2 Wuhan-1 and various variants. BSA was used as a negative control (MFI, mean fluorescence intensity).

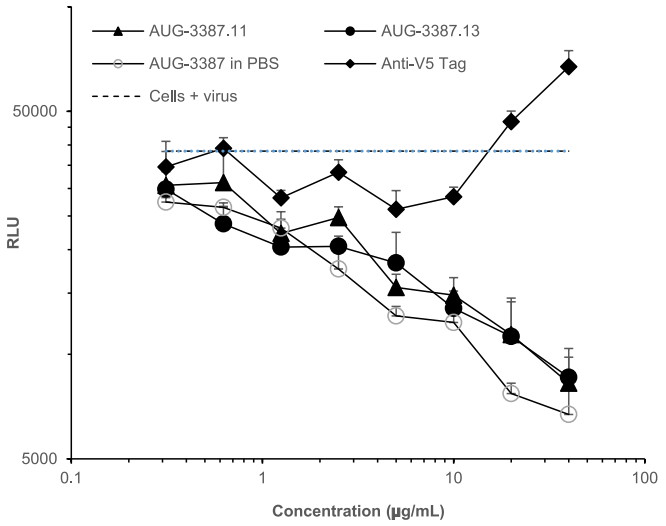

Fig. 3. Neutralization of Lenti pseudoviruses expressing SARS-CoV-2 Wuhan-1 spike RBD by AUG-3387, either as expressed in a PBS solution or reconstituted from TFF AUG-3387.11 or AUG-3387.13 powders (RLU, relative luminescence unit). The V5 Tag mAb (Anti-V5) was used as a negative control. Neutralization of the pseudoviruses led to the reduction of luciferase expression, indicated as RLU. No neutralization was expected in the Cells + Virus group. Data are mean ± S.D. (n = 3, 2 for the AUG-3387 in PBS). Comparison of values at all concentrations between AUG-3387 in PBS with AUG-3387.11 or with AUG-3387.13 using T-test showed p values larger than 0.05, except between AUG-3387 in PBS and AUG-3387.11 at 2.5 μg/mL.

indicating that the major polymorph of mannitol was changed from the beta form to delta form (Altay Benetti et al., 2021), after combining mannitol with other compositions in the TFF AUG-3387.11 powder. This observation by mDSC analysis agrees with the results from XRD analysis. No melting peak of sodium chloride was observed likely because its melting point was out of the testing range (Ferguson, 2002).

3.4. Feasibility of administering the TFF AUG-3387.11 powder directly into the lungs of Syrian hamsters to treat SARS-CoV-2 viral infection in the lungs

To test the feasibility of administering the TFF AUG-3387.11 powder directly into the lung to treat SARS-CoV-2 viral infection, we used the established hamster model (Driouich et al., 2023), pre-infected with SARS-CoV-2 viruses (i.e., intranasally inoculated 24 h before starting to administer the powder). Hamsters were given TFF AUG-3387.11 powder by IT insufflation at doses of 0.33 or 1 mg/kg, 24, 48, and 72 h after intranasal SARS-CoV-2 inoculation. As controls, hamsters were IP injected once 24 h after intranasal SARS-CoV-2 inoculation with an AUG-3387 in PBS solution at doses of 3.3 or 10 mg/kg or a vehicle control. The doses for the IT groups were set at 10 times lower than the doses for IP groups since the mAb powder was delivered directly into the lungs via IT administration, resulting in high local concentration in the lungs. All animals showed body weight loss, reaching maximum of 4–8 % 3–4 days after the viral inoculation and starting to recover on day 5. There were no apparent differences between the experiment groups in body weights, indicating that the TFF AUG-3387.11 powder at the specified dosing regimen was well tolerated when administered into the lungs. On day 5, animals were euthanized, and lung tissues were harvested. Lung weights and lung to body weight ratios were similar across all study groups ($p = 0.8624$ for lung weights, and 0.93 for lung to body weight ratios, ANOVA). Histopathology data showed that challenge of Syrian hamsters with SARS-CoV-2 via intranasal instillation resulted in mixed cell inflammation and associated epithelial hypertrophy/hyperplasia focused on the peribronchovascular and centriacinar areas of the lungs – the areas at the end of the conducting airways and the beginning of the gas exchange region. Except for the high dose TFF AUG-3387.11 powder given by IT insufflation, in which there was a limited suggestion of slightly lesser average severity in lung pathology for both gross pathology and light microscopy observations, animals in other groups demonstrated primary inflammatory change at levels that were generally like those seen in the Vehicle Control group. The viral load in the left lung tissues were assessed by RT-qPCR for subgenomic E gene RNA, which is generally considered a measurement of actively replicating virus. Although the high dose IP group trended toward significant viral load reduction, with subgenomic E gene RNA levels below the detection limit in 3 of the 6 hamsters, and the high dose IT group and low dose IP group each having one hamster with subgenomic E gene RNA level below the detection limit, there was no statistically significant difference among the experimental groups, unfortunately (Fig. 8), which is likely related to the large variations in the response (e.g., the relative standard variation (RSV) in the Vehicle Control group was 165 %) and the low number of animals per group ($n = 6$). Moreover, a significant difference could have been achieved if the experiment was designed for prevention, as for the treatment setting, the dosing regimen may need to be optimized. The sotrovimab administered by intramuscular injection at doses as high as 14 mg/kg three days prior to viral inoculation resulted in an improvement in body weight loss and a decreased viral load in the lung tissue as compared to control animals (Driouich et al., 2023), but there was not a report of data from a treatment setting for the antibody. Similarly, the casirivimab and imdevimab combination administered to hamsters by IP injection 24 h before viral inoculation resulted in a dose-dependent viral load reduction in lung tissues (Baum et al., 2020).

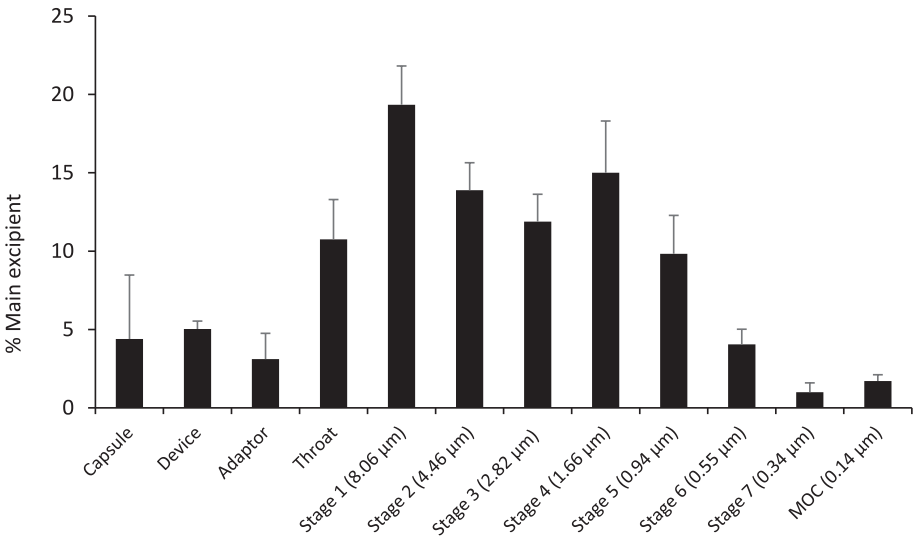

Fig. 4. Aerodynamic particle distribution of the TFF AUG-3387.11 powder in an NGI device after it was delivered using a RS00 high-resistance DPI (n = 3).

Table 3
Aerodynamic properties of the TFF AUG-3387.11 powder delivered using RS00 high-resistance DPI (n = 3).

	AUG-3387.11
MMAD (µm)	3.74 ± 0.73
GSD	2.73 ± 0.20
% FPF of recovered dose	46.36 ± 8.93
% FPF of delivered dose	50.95 ± 7.69
% Emitted fraction	90.58 ± 4.55

However, no change in viral load in the lung tissues was observed when the casirivimab and imdevimab combination was IP injected 24 h after viral inoculation in a manner similar to our study, although a benefit in animal weights was clear in the high dose groups (i.e., 50 mg/kg and 5 mg/kg) (Baum et al., 2020), likely due to the low availability of systemically injected mAbs to lung tissues and the long time it took for a sufficient amount of the mAbs to reach the lung tissues, especially to the epithelial cells infected by the viruses in the early stage of the infection (Lai et al., 2021). Directly delivering the mAbs into the lungs by IT insufflation (or oral inhalation if in a human subject) is different, as the mAbs immediately had access to viruses in the bronchoalveolar fluid to bind them, preventing them from entering the epithelial cells.

Finally, it is noted that although the AUG-3387 mAb reconstituted from the TFF AUG-3387.11 powder did not show detectable difference in its ability to bind to SARS-CoV-2 RBDs and neutralize SARS-CoV-2 Wuhan-1 RBD-expressing pseudoviruses as compared to the original AUG-3387 in a PBS solution (Figs. 1–3), the powder composition likely has room to improve. Mannitol is not an ideal excipient to stabilize proteins during freeze-drying, although it is commonly used as a bulking agent (Kim et al., 1998). Also, the excipients in the TFF AUG-3387.11 powder, mannitol, leucine, and salts in the PBS buffer, were all predominately in crystalline form (Figs. 6 and 7), making long-term storage a challenge (Arte et al., 2024). A key reason that the TFF AUG-3387.11 powder was used at the time (i.e., back during the COVID-19 pandemic) in the hamster study was that the mannitol, the main inactive ingredient in the powder, is in Bronchitol®, an FDA-approved inhaled dry powder formation indicated as an add-on maintenance therapy in patients with cystic fibrosis (FDA). We have since prepared other TFF powders of the AUG-3387 with different compositions with more desirable physical and aerosol properties that contained a histidine buffer instead of PBS, Tween 20 or Tween 80 as a surface active agent, trehalose, and polymers such as cyclodextrin (Yu et al., 2023). For example, a TFF AUG-3387 powder that contained trehalose, hydroxypropyl-β-cyclodextrin, leucine, and Tween 80 had minimal high molecular weight (HMW) species and subvisible aggregates, with the AUG-3387 mAbs being embedded in an amorphous glass with a glass transition temperature (Tg) of ~119 °C (Sahakijjpijarn and Owens, unpublished data). This TFF AUG-3387 powder likely has advantages over the TFF AUG-3387.11 powder in certain aspects such as storage stability, but it is not without shortcomings. For example, the use of cyclodextrin in an inhaled product may raise long-term safety concerns (Hussain et al., 2004). While it was reported the short-term exposure to inhaled cyclodextrin derivatives only caused a slight increase in lymphocyte counts in

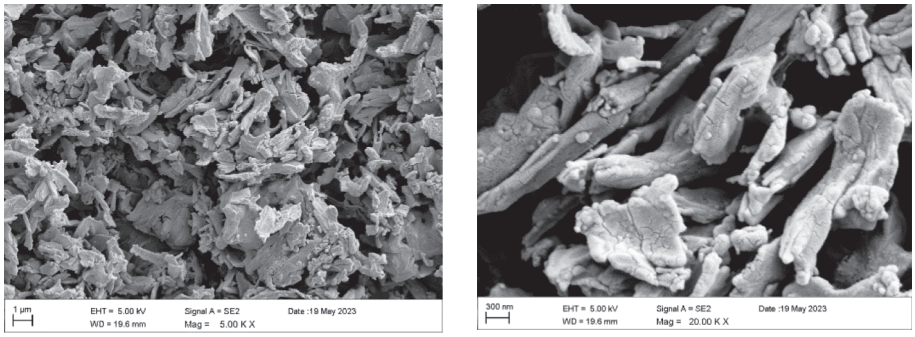

Fig. 5. Representative SEM images of the TFF AUG-3387.11 powder.

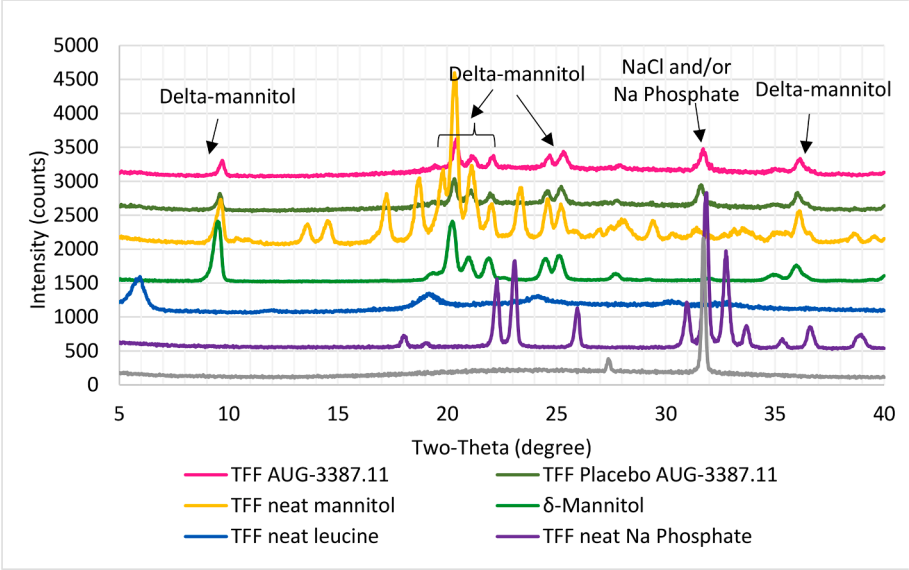

Fig. 6. XRD diffractograms of the TFF AUG-3387.11 powder and its excipients.

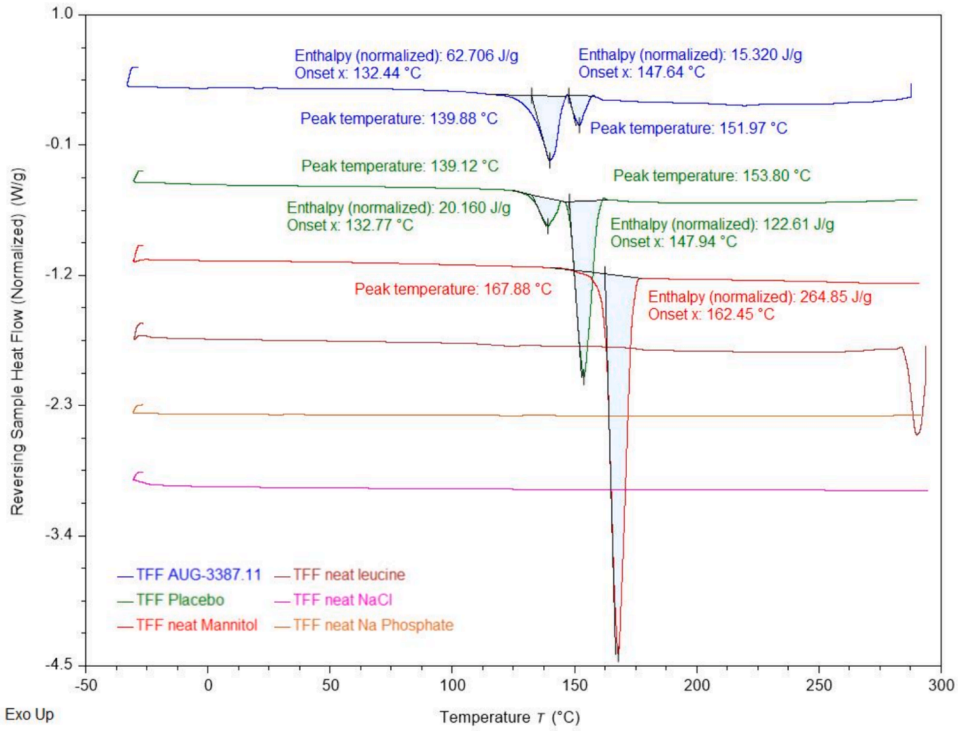

Fig. 7. MDSC curves of TFF AUG-3387.11 powder and its excipients.

bronchoalveolar lavage fluid (Evrard et al., 2004), cyclodextrins can act as an adsorption enhancer of proteins (Depreter et al., 2013), which may irreversibly disrupt the alveolar epithelial cell layer (Hussain et al., 2004). As a result, the lungs can be more susceptible to exogenous allergens and dust particles that are inhaled during respiration (Hussain et al., 2004). Therefore, for a given mAb that one intends to develop into a clinical inhaled dry powder product using the TFFD process, more formulation and composition optimization will likely be needed. Nonetheless, data shown in Figs. 1–5 demonstrated that it is feasible to apply the TFFD process to convert a virus-neutralizing mAb into pharmacologically active dry powders with desirable aerosol properties for pulmonary delivery.

4. Conclusions

Using AUG-3387, a human-derived mAb that binds to various SARS-CoV-2 RBD variants, as a model mAb, we demonstrated that dry powder formulations of the mAb prepared using the TFFD process retained the full binding ability and virus-neutralizing activity of the mAb. The mAb powders have desirable aerosol properties for direct delivery into the lungs for potential reduction of local SARS-CoV-2 viral load.

CRediT authorship contribution statement

Haiyue Xu: Writing – original draft, Methodology, Investigation,

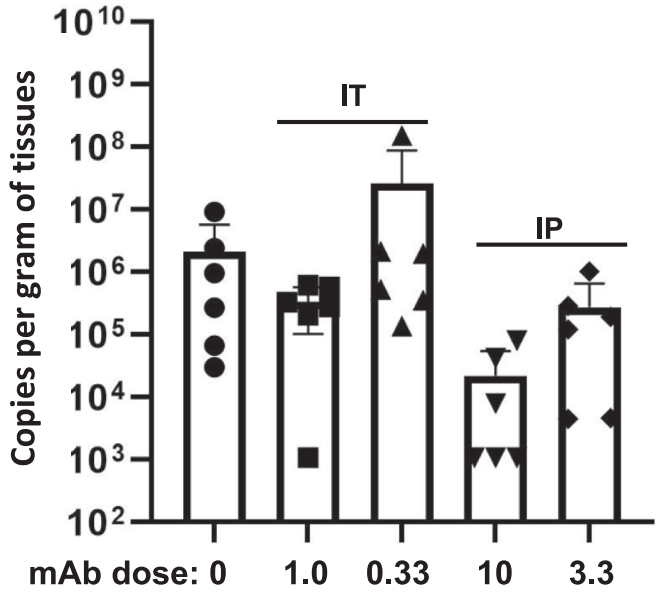

Fig. 8. SARS-CoV-2 viral subgenomic RNA levels in Syrian hamster lung tissues after intraperitoneal injection of an AUG-3387 solution (IP) or intratracheal insufflation of the TFF AUG-3387.11 powder (IT) one day after the hamsters were intranasally inoculated with SARS-CoV-2 viruses. The mAb dose of 0 represents the Vehicle Control group. Data are mean ± S.E.M. (n = 6).

Formal analysis, Data curation. **Sawittree Sahakijpijarn:** Writing – original draft, Methodology, Investigation, Formal analysis, Data curation. **Chaeho Moon:** Methodology, Investigation, Formal analysis, Data curation. **Christopher J. Emig:** Writing – review & editing, Supervision, Resources, Project administration, Funding acquisition, Formal analysis, Conceptualization. **Marco Mena:** Methodology, Investigation, Formal analysis, Data curation. **Steven J. Henry:** Methodology, Investigation, Formal analysis, Data curation. **Adela Vitug:** Methodology, Investigation, Formal analysis, Data curation. **Christian John Ventura:** Methodology, Investigation, Formal analysis, Data curation. **Philip J. Kuehl:** Supervision, Project administration, Methodology, Investigation, Formal analysis, Data curation. **David Revelli:** Methodology, Investigation, Formal analysis, Data curation. **Donald E. Owens:** Writing – review & editing, Supervision, Project administration. **Dale J. Christensen:** Writing – review & editing, Supervision, Resources, Project administration, Conceptualization. **Robert O. Williams:** Writing – review & editing, Resources, Funding acquisition, Conceptualization. **Zhengrong Cui:** Writing – review & editing, Supervision, Resources, Project administration, Funding acquisition, Conceptualization.

Declaration of competing interest

The authors declare the following financial interests/personal relationships which may be considered as potential competing interests: Cui reports a relationship with TFF Pharmaceuticals, Inc. that includes: equity or stocks and funding grants. Williams reports a relationship with TFF Pharmaceuticals, Inc. that includes: consulting or advisory, equity or stocks, and funding grants. Xu and Moon report a relationship with TFF Pharmaceuticals, Inc. that includes: consulting or advisory. Cui, Williams, Christensen, Emig, Mena, Vitug and Henry are inventors on IP related to this work. Christensen was a consultant for TFF Pharmaceuticals. Emig, Mena, Vitug, Henry, and Ventura are or were employees of Augmenta Bioworks, Inc. ZC serves as the Editor of the International Journal of Pharmaceutics for North America. This paper was subject to all the Journal's usual procedures. The peer review was handled, and the editorial decision was made independently of ZC and his research group.

Data availability

Data will be made available on request.

Acknowledgements

This work was supported in part by TFF Pharmaceuticals, Inc. and Augmenta Bioworks, Inc.

References

Altay Benetti, A., et al., 2021. Mannitol polymorphs as carrier in DPIs formulations: isolation characterization and performance. Pharmaceutics 13 (8).
Arte, K.S., et al., 2024. Understanding the impact of mannitol on physical stability and aerosolization of spray-dried protein powders for inhalation. Int. J. Pharm. 650, 123698.
Baum, A., et al., 2020. REGN-COV2 antibodies prevent and treat SARS-CoV-2 infection in rhesus macaques and hamsters. Science 370 (6520), 1110–1115.
Brainerd, C.J., et al., 2023. How does attribute ambiguity improve memory? Mem. Cognit. 51 (1), 38–70.
Chen, P., et al., 2021. SARS-CoV-2 neutralizing antibody LY-CoV555 in outpatients with Covid-19. N. Engl. J. Med. 384 (3), 229–237.
Crowe Jr, J.E., et al., 1994. Recombinant human respiratory syncytial virus (RSV) monoclonal antibody Fab is effective therapeutically when introduced directly into the lungs of RSV-infected mice. PNAS 91 (4), 1386–1390.
Crowe Jr, J.E., et al., 1998. Isolation of a second recombinant human respiratory syncytial virus monoclonal antibody fragment (Fab RSVF2-5) that exhibits therapeutic efficacy in vivo. J. Infect. Dis. 177 (4), 1073–1076.
Depreter, F., Pilcer, G., Amighi, K., 2013. Inhaled proteins: Challenges and perspectives. Int. J. Pharm. 447 (1), 251–280.
Detalle, L., et al., 2016. Generation and characterization of ALX-0171, a potent novel therapeutic nanobody for the treatment of respiratory syncytial virus infection. Antimicrob. Agents Chemother. 60 (1), 6–13.
Driouich, J.S., et al., 2023. Activity of Sotrovimab against BQ.1.1 and XBB.1 Omicron sublineages in a hamster model. Antiviral Res.. 215, 105638.
Emig, C.J.M., A., M., Henry, S.J., Vitug, A., Ventura, C.J., Fox, D., Nguyenla, X.H., Xu, H., Moon, C., Sahakijjpijarn, S., Keuhl, P.J., Revelli, D., Cui, Z., Williams III, R.O., Christensen, D.J., 2021. AUG-3387, a human-derived monoclonal antibody neutralizes SARS-CoV-2 variants and reduces viral load from therapeutic treatment of hamsters in vivo. BioRxiv. https://doi.org/10.1101/2021.10.12.464150.
Evrard, B., et al., 2004. Cyclodextrins as a potential carrier in drug nebulization. J. Control. Release 96 (3), 403–410.
FDA, Bronchitol prescribing information.
Ferguson, J.B., 2002. The melting and freezing point of Sodium Chloride. J. Phys. Chem. 26 (7), 626–630.
Gupta, A., et al., 2021. Early treatment for Covid-19 with SARS-CoV-2 neutralizing antibody sotrovimab. N. Engl. J. Med. 385 (21), 1941–1950.
Hermet, P., et al., 2023. Broadly neutralizing humanized SARS-CoV-2 antibody binds to a conserved epitope on Spike and provides antiviral protection through inhalation-based delivery in non-human primates. PLoS Pathog. 19 (8), e1011532.
Hou, Y.J., et al., 2020. SARS-CoV-2 reverse genetics reveals a variable infection gradient in the respiratory tract. Cell 182 (2), 429–446 e14.
Hufnagel, S., et al., 2022a. The development of thin-film freezing and its application to improve delivery of biologics as dry powder aerosols. Kona Powder Part. J. 2022010.
Hufnagel, S., et al., 2022b. Dry powders for inhalation containing monoclonal antibodies made by thin-film freeze-drying. Int. J. Pharm. 618, 121637.
Hussain, A., et al., 2004. Absorption enhancers in pulmonary protein delivery. J. Control. Release 94 (1), 15–24.
Kim, A.I., Akers, M.J., Nail, S.L., 1998. The physical state of mannitol after freeze-drying: effects of mannitol concentration, freezing rate, and a noncrystallizing cosolute. J. Pharm. Sci. 87 (8), 931–935.
Lai, S.K., McSweeney, M.D., Pickles, R.J., 2021. Learning from past failures: challenges with monoclonal antibody therapies for COVID-19. J. Control Release 329, 87–95.
Leyva-Grado, V.H., et al., 2015. Direct administration in the respiratory tract improves efficacy of broadly neutralizing anti-influenza virus monoclonal antibodies. Antimicrob. Agents Chemother. 59 (7), 4162–4172.
Maranda, B., et al., 2024. Safety and efficacy of inhaled IBIO123 for mild-to-moderate COVID-19: a randomised, double-blind, dose-ascending, placebo-controlled, phase 1/2 trial. Lancet Infect. Dis. 24 (1), 25–35.
McBride, J.M., et al., 2017. Phase 2 randomized trial of the safety and efficacy of MHAA4549A, a broadly neutralizing monoclonal antibody, in a human influenza A virus challenge model. Antimicrob. Agents Chemother. 61 (11).
Moon, C., et al., 2019. Processing design space is critical for voriconazole nanoaggregates for dry powder inhalation produced by thin film freezing. J. Drug Deliv. Sci. Technol. 54.
Moon, C., et al., 2019. Enhanced aerosolization of high potency nanoaggregates of voriconazole by dry powder inhalation. Mol. Pharm. 16 (5), 1799–1812.
Overhoff, K.A., et al., 2009. Use of thin film freezing to enable drug delivery: a review. J. Drug Deliv. Sci. Technol. 19 (2), 89–98.
Piepenbrink, M.S., et al., 2021. Therapeutic activity of an inhaled potent SARS-CoV-2 neutralizing human monoclonal antibody in hamsters. Cell Rep. Med. 2 (3), 100218.

Prince, G.A., et al., 1987. Effectiveness of topically administered neutralizing antibodies in experimental immunotherapy of respiratory syncytial virus infection in cotton rats. J. Virol. 61 (6), 1851–1854.
Reed, L.J., Muench, H., 1938. A simple method of estimating fifty per cent endpoints. Am. J. Epidemiol. 27 (3), 493–497.
Sahakijpijarn, S., et al., 2020. Using thin film freezing to minimize excipients in inhalable tacrolimus dry powder formulations. Int. J. Pharm. 586, 119490.
Seow, H.C., et al., 2023. Neutralisation of SARS-CoV-2 by monoclonal antibody through dual targeting powder formulation. J. Control. Release 358, 128–141.
Streblow, D.N., et al., 2023. Aerosol delivery of SARS-CoV-2 human monoclonal antibodies in macaques limits viral replication and lung pathology. Nat. Commun. 14 (1), 7062.
Wang, Y.B., Watts, A.B., Williams, R.O., 2014. Effect of processing parameters on the physicochemical and aerodynamic properties of respirable brittle matrix powders. J. Drug Deliv. Sci. Technol. 24 (4), 390–396.
Watts, A.B., et al., 2013. Respirable low-density microparticles formed in situ from aerosolized brittle matrices. Pharm. Res. 30 (3), 813–825.
Weinreich, D.M., et al., 2021. REGN-COV2, a neutralizing antibody cocktail, in outpatients with Covid-19. N. Engl. J. Med. 384 (3), 238–251.
Xu, X., et al., 2020. Evolution of the novel coronavirus from the ongoing Wuhan outbreak and modeling of its spike protein for risk of human transmission. Sci. China Life Sci. 63 (3), 457–460.
Yu, Y.S., et al., 2023. Feasibility of intranasal delivery of thin-film freeze-dried, mucoadhesive vaccine powders. Int. J. Pharm. 640, 122990.